



## Thermally cross-linkable spirobifluorene-core-based hole transport layer with high solvent-resistivity for solution processible OLEDs

Young Eun Kim<sup>a,1</sup>, Ara Ko<sup>a,1</sup>, Ho Jin Jang<sup>a</sup>, Sung Joon Yoon<sup>a</sup>, Seung Hun Roh<sup>a</sup>, Jun Young Lee<sup>a</sup>, Jun Yeob Lee<sup>a</sup>, Dukjoon Kim<sup>a,\*\*</sup>, Jung Kyu Kim<sup>a,\*</sup>, Kyoung Soo Yook<sup>a,b,\*\*\*</sup>

<sup>a</sup> School of Chemical Engineering, Sungkyunkwan University (SKKU), Suwon, 16419, Republic of Korea

<sup>b</sup> CYNORA GmbH, Werner-von-Siemensstraße 2-6, Building 5110, 76646, Bruchsal, Germany

### ARTICLE INFO

#### Keywords:

Thermal crosslinking  
Hole transport layer  
Solvent-resistivity  
Solution processible OLED  
Multi-layer coating

### ABSTRACT

The fabrication of organic light-emitting diodes (OLEDs) composed of multi-layered structure through a solution-based process suffers from the dissolution of the preformed lower parts during the coating of upper layers. To prevent this problem during the solution process, a promising approach of introducing a cross-linkable layer with a high solvent-resistivity has been proposed. Herein, thermally cross-linkable spirobifluorene-core-incorporated hole transport layers (HTLs) with a cross-linking temperature of 180 °C are designed for solution-processible OLEDs composed of multi-layered structures. The enhanced morphology stability and solvent-resistive property of the synthesized HTLs are evaluated through a rinsing-test with an organic solvent used for the emitting layer. Considering the charge transport property of HTLs in OLEDs, the appropriate energy level and triplet energy values of the synthesized HTLs promote the efficient cascade hole migration. Consequently, the OLED composed of thermally cross-linkable HTL shows higher quantum efficiency (QE) of 16.5% and lower operation voltage of 5.1 V at 1000 cd/m<sup>2</sup>, compared to that composed of a commercialized polymer, poly (9-vinyl-carbazole) (PVK). Thus, in this study, the feasibility of the potential application of thermally cross-linkable HTL with the spirobifluorene-core-units as charge transport layers for solution-based optoelectronic devices composed of multi-layered structures has been verified.

### 1. Introduction

In recent decades, organic light-emitting diodes (OLEDs) have been extensively developed and studied due to the rapid increase in their demand by display and lighting industries. This swift heightened demand is due to their numerous advantages such as lightweight, low operating potential, fast response, and large area processibility with low cost [1–6]. OLEDs with a high quantum efficiency (QE) can be fabricated using a thermal evaporation process. Such a process occurs within a high vacuum chamber and is widely used to obtain multi-layered structures with fine morphology and thickness of few-tens nanometers [7–10]. However, the use of a high-vacuum-based evaporation process for the deposition of organic materials suffers from restricted scalability, limited choice of materials, and high operating cost [10–13]. To resolve the aforementioned issues, solution-based wet processes such as

roll-to-roll, ink-jet, and screen printing processes have drawn considerable attention due to their promising features for the fabrication of large-area OLEDs with low cost [14–16]. Solution-based wet processes are highly feasible for the fabrication of flexible or wearable devices [17]. However, the main challenge of the solution-based wet process in fabricating OLEDs with a multi-layered structure is the prevention of the dissolution of lower parts during the coating process [18,19]. The formerly coated organic layers on transparent conductive oxide (TCO) substrates such as indium tin oxide (ITO) glass have good solubility in the organic solvent of the upper layer such as chlorobenzene. Hence, the deposition of the emitting layer (EML) with the solution-based wet process can damage the lower layers and severely distort their morphology [19].

The use of cross-linkable charge-transporting layers has been considered as a promising approach to resolve the dissolution issue

\* Corresponding author.

\*\* Corresponding author. School of Chemical Engineering, Sungkyunkwan University (SKKU), Suwon, 16419, Republic of Korea.

\*\*\* Corresponding author. School of Chemical Engineering, Sungkyunkwan University (SKKU), Suwon, 16419, Republic of Korea.

E-mail addresses: [djkim@skku.edu](mailto:djkim@skku.edu) (D. Kim), [legkim@skku.edu](mailto:legkim@skku.edu) (J.K. Kim), [yook@cynora.com](mailto:yook@cynora.com) (K.S. Yook).

<sup>1</sup> Y. E. Kim and A. Ko contributed equally in this work.

during the solution-based wet process [20]. After the deposition of the cross-linkable material, the cross-linking process is conducted to improve its solvent-resistive property and morphology stability, thereby successfully achieving a multi-layered structure over the crosslinked layer. Recently, cross-linkable materials comprising of thermally cross-linked units or moieties are widely adapted to the hole transport layer (HTL) of OLEDs. In comparison to a photo-assisted cross-linkable HTL, the thermally cross-linkable HTL is free from undesired contaminants or residuals originating from cross-linking agents which may deteriorate the device performance [17,21]. To obtain a robust HTL, an annealing process is required for the thermally cross-linkable materials without harnessing any additional agents or additives in the HTL. However, the challenges involved with the use of cross-linkable HTLs are high annealing temperatures of over 200 °C and undesired changes in film morphology which results in thermal stress.

Herein, thermally cross-linkable spirobifluorene-core-incorporated HTLs were synthesized for the fabrication of solution-processible OLEDs. The two synthesized compounds, N-phenyl-7-(4-(2-(phenyl(4-((4-vinylbenzyl)oxy)phenyl)amino)-9,9'-spirobifluorene)-7-yl)phenyl)-N-(4-((4-vinylbenzyl)oxy)phenyl)amino)-9,9'-spirobifluorene-2-amine (hereafter, DSP) and N-phenyl-7-(4'-(2-(phenyl(4-((4-vinylbenzyl)oxy)phenyl)amino)-9,9'-spirobifluorene)-7-yl)-[1,1'-biphenyl]-4-yl)-N-(4-((4-vinylbenzyl)oxy)phenyl)amino)-9,9'-spirobifluorene-2-amine (hereafter, DSBP) were spin-coated on the HTL comprised of poly(3,4-ethylenedioxythiophene):poly(styrenesulfonate) (PEDOT:PSS). The thermal annealing process for the cross-linking of the HTL was carried out at a temperature of 180 °C as determined from the differential scanning calorimetry (DSC) and thermogravimetry (TG) analysis. The enhanced morphology stability and solvent-resistive property of DSBP in comparison with that of DSP were evaluated via a rinsing-test with an organic solvent. These properties were investigated by the ultraviolet (UV)-vis absorption spectra and the atomic force microscopy (AFM). The synthesized HTLs were used to fabricate OLEDs with a multi-layered structure consisting of ITO glass, hole injection layer (HIL), HTL, EML, electron transport layer (ETL), and lithium fluoride/aluminum (LiF/Al). To compare the performance of the device, a device composed of a commercialized polymer, poly(9-vinylcarbazole) (PVK), as the HTL was fabricated. Considering the charge transport property of the HTL, the efficient cascade hole migration was expected in the DSP and DSBP compared to PVK due to the presence of appropriate energy levels and triplet energy values. Consequently, the OLEDs composed of DSBP had the highest maximum QE of 16.5%, compared to that of the OLEDs composed of DSP and PVK, 15.0% and 11.9%, respectively. Furthermore, the use of DSBP induced a lower operating voltage of 5.1 V at 1000 cd/m<sup>2</sup>, compared to that of the OLEDs with DSP and PVK, 5.5 and 6.0 V, respectively. More importantly, in aspect of OLEDs fabrication process, cross-linkable hole transport layer with spirobifluorene-core-units can be efficiently utilized in various solution-based optoelectronic devices due to the enhancement of solvent-resistive property and thermal stability of structure.

## 2. Experimental section

### 2.1. Materials

4-bromo-butene, 1,3,5-tribromobenzene, 4-(dimethylamino)pyridine, ditert-butyl dicarbonate, diphenylamine, trifluoroacetic acid, tribromoborane, bis(4-methoxyphenyl)amine, bis(4-methoxyphenyl)amine, 4-vinylbenzyl chloride, acetonitrile and 1,1'-Ferrocenediyl-bis(diphenylphosphine) (DPPF) were purchased from Sigma Aldrich Chem. Co., Korea. Sodium *tert*-butoxide and 3,6-dimethoxy-9H-carbazole were purchased from Alfa Aesar Chem. Co. and TCI Chem. Co., respectively. Palladium (0) acetate, tris(dibenzylideneacetone)dipalladium (0) were purchased from P&H Tech. Co. Sodium hydroxide, potassium carbonate (K<sub>2</sub>CO<sub>3</sub>), dimethylformamide (DMF), acetone, and potassium phosphate were purchased from Duksan Sci. Co., Korea. Dichloromethane

(CH<sub>2</sub>Cl<sub>2</sub>), DMF, and acetone were purchased from Daejung Sci. Co., Korea. Toluene and tetrahydrofuran (THF) (obtained from Sigma Aldrich Chem. Co., Korea) were purified with calcium hydride and sodium. Poly(3,4-ethylenedioxythiophene):poly(styrenesulfonate) (PEDOT:PSS, CLEVIOS™ P VP Al 4083, Heraeus) was used for the HIL.

### 2.2. Device fabrication

The patterned ITO substrates were cleaned via ultra-sonication for 10 min each in acetone, distilled water, and IPA, sequentially. Subsequently, the substrate was treated with UV ozone treatment. The HIL, HTL, and EML were deposited on the surface of the cleaned ITO substrate via a spin-coating process at a rotational speed of 2000 rpm for 25 s. For the HTL, the hole transport materials (HTMs) were dissolved in 0.3 wt % chloroform. After the spin-coating of the HTMs at 2000 rpm for 25 s, the thermal treatment was carried out on a hot plate at 200 °C for 30 min to crosslink the HTMs. For the EML, (Tris(4-carbazoyl-9-yl)phenyl)amine (TCTA) and 3-(3-(carbazole-9-yl)phenyl)pyrido[3',2':4,5]furo[2,3-b]pyridine (3Cz-PFP) were dissolved in 0.7 wt % toluene, which was used for the mixed host of the EML with a 9:1 ratio. Also, Ir(mppy)<sub>3</sub> was dissolved in 0.2 wt % toluene and doped in the mixed host with 10% doping concentration. After the spin-coating of the EML, the solvent drying was performed on the hot plate at 80 °C for 20 min. The TPBi (ETL), LiF, and Al cathode were deposited in a thermal vacuum deposition chamber with vacuum pressure under 10<sup>-7</sup> torr. The rate of vacuum deposition was 1 Å/s for the ETL, 0.1 Å/s for LiF, and 1 Å/s for the Al cathode [22]. The fabricated devices were encapsulated by using glass lids, calcium oxide (CaO) getters, and epoxy resin to prevent moisture and oxygen penetration [23]. The epoxy resin was cured under UV light irradiation with 254 nm wavelength by an x-light 400p UV lamp for 25 s. Consequently, the green OLEDs were fabricated with the following structure: ITO/PEDOT:PSS(35 nm)/HTMs (20–25 nm)/TCTA:3CzPFP:Ir(mppy)<sub>3</sub> (30 nm)/TPBi(35 nm)/LiF(1 nm)/Al (200 nm).

### 2.3. Characterizations

High-resolution hydrogen-1 nuclear magnetic resonance (1H NMR) spectra were measured by a UNITY INOVA 500 spectrometer (Varian, Inc., USA), operated at 500 MHz to analyse the chemical structure of the compounds. Gas chromatography high resolution mass spectroscopy (GC-HRMS) was obtained using a JEOL, JMS-700. Atmospheric Solids Analysis Probe (ASAP) mass spectrometry (MS) experiment was conducted to obtain the mass spectra with high resolution. The performance of the OLED devices including the external quantum efficiency (EQE), current efficiency (CE), electroluminescence (EL) spectra, current density, and luminance was measured using a Keithley 2400 source measurement unit and CS-2000 spectroradiometer. The UV-Vis absorption spectra of the synthesized compounds were measured using a JASCO V-730 UV-Vis spectrometer. To investigate the UV-Vis spectra, the synthesized compounds were dissolved in their solvents with the concentration of 1 × 10<sup>-5</sup> mol/L [24,25]. The PL spectra of the synthesized compounds were measured using a PerkinElmer LS55 fluorescence spectrophotometer in solution, solid-state [26]. As before, the compounds were dissolved in anhydrous toluene and THF depending on the degree of dissolution and then dispersed in 1 wt % polystyrene (PS) to get solid samples. The low-temperature PL spectra were measured at 77 K with liquid nitrogen and with the delay time set to determine the value of the triplet energy. The highest occupied molecular orbital (HOMO) energy level of the synthesized compounds was measured by cyclic voltammetry (CV) (IviumStat.h, IVIUM Tech. Netherlands) with a scan rate of 0.1 V/s. The glassy carbon electrode, Ag/AgCl electrode, and Pt wire were used as the working, reference, and counter electrodes, respectively. 0.1 M tetrabutylammonium perchlorate was used for the electrolyte. To obtain the correction values, ferrocene and 1,3-Bis(N-carbazoyl)benzene (mCP) (obtained from Sigma Aldrich Chem. Co., Korea)

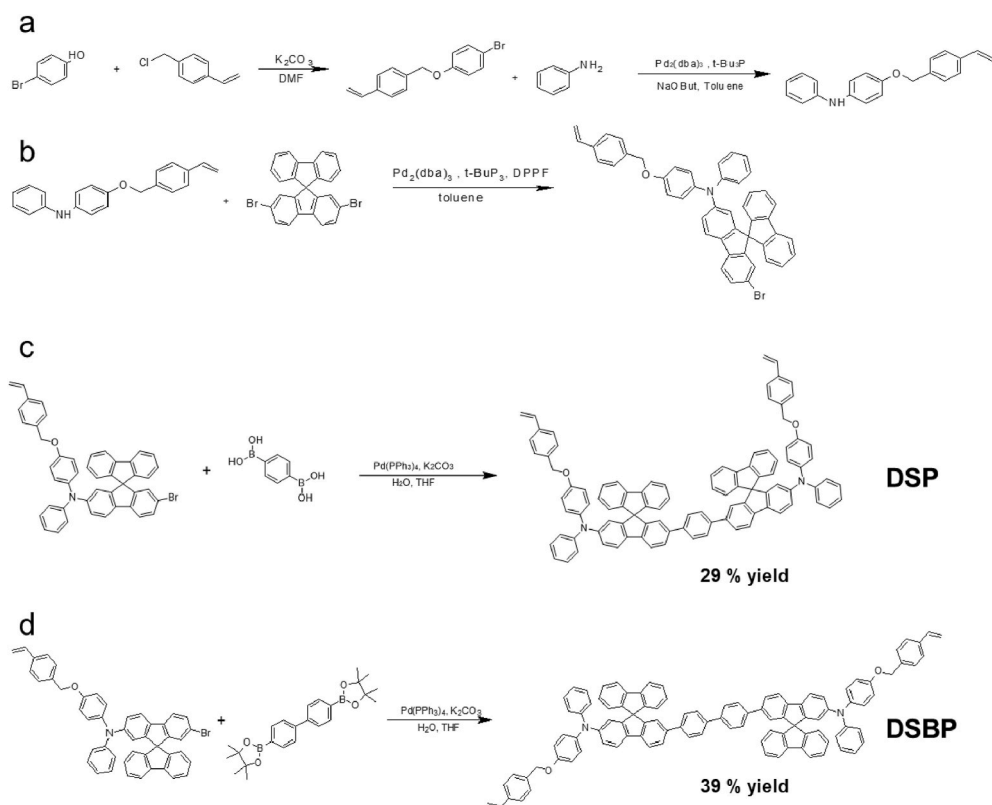


**Fig. 1.** Synthesis scheme (a) N-phenyl-4-((4-vinylbenzyl)oxy)aniline, (b) 7-bromo-N-phenyl-N-(4-((4-vinylbenzyl)oxy)phenyl)-9,9'-spirobi [fluoren]-2-amine, (c) DSP, and (d) DSBP.

were used as the comparative materials. For the DSC analysis, the exothermal and endothermal peaks of the synthesized compounds were measured by TA Instruments DSC Q2000 with a heating rate of 10 °C/min for two cycles. The 2nd scan was started after cooling from over 350 °C to room temperature. For the TGA, the decomposition temperature of the synthesized compounds was measured using a Seiko Exstar 6000 with a decreasing heating rate of 10 °C/min from room temperature to 600 °C. The decomposition temperature ( $T_d$ ) was detected at the starting point of the slope of the curve of weight loss with time. The surface morphology of films was investigated via AFM. The Fourier transform infrared (FT-IR) spectra of the synthesized compounds were measured by a Bruker IFS-66/S within the wavenumber scan range of 4000–400  $\text{cm}^{-1}$ . For the FT-IR spectroscopy, the compounds were dissolved in toluene and drop-casted on Si-wafer substrates.

### 3. Results and discussion

The synthesis schemes of N-phenyl-7-(4-(2-(phenyl(4-((4-vinylbenzyl)oxy)phenyl)amino)-9,9'-spirobi [fluoren]-7-yl)phenyl)-N-(4-((4-vinylbenzyl)oxy)phenyl)amino)-9,9'-spirobi [fluoren]-2-amine (DSP) and N-phenyl-7-(4'-(2-(phenyl(4-((4-vinylbenzyl)oxy)phenyl)amino)-9,9'-spirobi [fluoren]-7-yl)-[1,1'-biphenyl]-4-yl)-N-(4-(4-vinylbenzyl)oxy)phenyl)amino)-9,9'-spirobi [fluoren]-2-amine (DSBP) are displayed in Fig. 1. The detailed synthesis protocol of 1-bromo-4-((4-vinylbenzyl)oxy)benzene, N-phenyl-4-((4-vinylbenzyl)oxy)aniline, and 7-bromo-N-phenyl-N-(4-((4-vinylbenzyl)oxy)phenyl)-9,9'-spirobi [fluoren]-2-amine are described in the supplementary information. For the synthesis of DSP, 7-bromo-N-phenyl-N-(4-((4-vinylbenzyl)oxy)phenyl)-9,9'-spirobi [fluoren]-2-amine (3 g, 4.32 mmol) and 1,4-phenylenediboric acid (0.32 g, 2 mmol) were dissolved in distilled THF (10 ml). Tetrakis (triphenylphosphine)palladium (0) (0.06 g, 0.05 mmol) and 2 M aqueous  $\text{K}_2\text{CO}_3$  (5 ml) were added into the reaction mixture and stirred overnight. At the completion of the reaction, the product was extracted

with  $\text{CH}_2\text{Cl}_2$  and distilled water, and the organic layer was dried over magnesium sulphate ( $\text{MgSO}_4$ ) and concentrated after filtering. The concentrated reaction product was purified using a silica gel column using dichloromethane/hexane (1/5, v/v) as the eluent. The yellowish white solid product was obtained. The weight of the purified product obtained was 0.9 g (29% yield).  $^1\text{H}$  NMR (500 MHz,  $\text{CDCl}_3$ , ppm):  $\delta$  7.33 (dd,  $J = 7.8, 2.8$  Hz, 4H), 7.63 (d,  $J = 8.3$  Hz, 1H), 7.51 (dd,  $J = 8.0, 1.6$  Hz, 1H), 7.44–7.27 (m, 11H), 7.17–7.01 (m, 6H), 6.966.66 (m, 16H), 6.50 (s, 1H), 5.75 (dd,  $J = 17.6, 0.7$  Hz, 1H), 5.31–5.23 (m, 5H), 4.95 (s, 2H), 3.74 (ddd,  $J = 6.6, 3.4, 1.6$  Hz, 6H), 1.89–1.80 (m, 6H), 1.55 (s, 4H), 1.26 (d,  $J = 15.4$  Hz, 2H), 1.03–0.75 (m, 2H).  $^{13}\text{C}$  NMR (125 MHz,  $\text{CDCl}_3$ , ppm):  $\delta$  207.10, 137.55, 136.87, 136.67, 129.97, 127.93, 127.35, 126.70, 236.63, 114.30. GC-HRMS (FAB+)  $m/z$  1304.5291 [(M + H)+]; Calcd. For  $\text{C}_{98}\text{H}_{68}\text{N}_2\text{O}_2$ , 1304.5281. For the synthesis of DSBP, 7-bromo-N-phenyl-N-(4-((4-vinylbenzyl)oxy)phenyl)-9,9'-spirobi [fluoren]-2-amine (3 g, 4.32 mmol) and 4,4'-Biphenyldiboric acid (0.48 g, 2 mmol) were dissolved in distilled THF (10 ml). Tetrakis (triphenylphosphine)palladium (0) (0.06 g, 0.05 mmol) and 2 M aqueous  $\text{K}_2\text{CO}_3$  (5 ml) were added into the reaction mixture and stirred overnight. After the reaction was completed, the reaction product was extracted with  $\text{CH}_2\text{Cl}_2$  and distilled water, and the organic layer was dried over  $\text{MgSO}_4$  and concentrated after filtering. The concentrated reaction product was purified by silica gel column using dichloromethane/hexane (1/5, v/v) as the eluent. The yellowish white solid product was obtained solid product was obtained. The weight of the purified product obtained was 1.03 g (39% yield).  $^1\text{H}$  NMR (500 MHz,  $\text{CDCl}_3$ , ppm):  $\delta$  7.76 (t,  $J = 8.4$  Hz, 4H), 7.66 (d,  $J = 7.9$  Hz, 1H), 7.58 (dd,  $J = 8.0, 1.6$  Hz, 1H), 7.43 (m, 12H), 7.31 (td,  $J = 7.5, 1.0$  Hz, 3H), 7.13–7.01 (m, 6H), 7.00–6.67 (m, 18H), 6.51 (s, 1H), 5.76 (dd,  $J = 17.6, 0.8$  Hz, 1H), 5.34–5.19 (m, 5H), 4.96 (s, 3H), 3.81–3.63 (m, 4H), 1.91–1.75 (m, 4H), 1.55 (s, 3H), 1.37–1.20 (m, 4H), 0.88 (dd,  $J = 8.6, 5.4$  Hz, 2H). GC-HRMS (FAB+)  $m/z$  1380.5600 [(M + H)+]; Calcd. For  $\text{C}_{104}\text{H}_{72}\text{N}_2\text{O}_2$ , 1380.5594. The  $^1\text{H}$  NMR spectra were displayed in Fig. S1, supporting information.

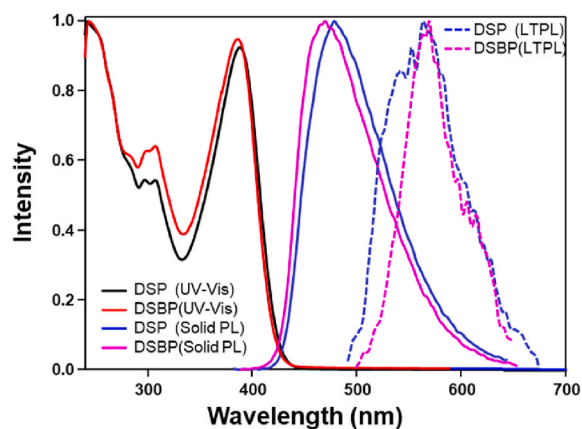


Fig. 2. UV-Vis absorbance and PL spectra, and Low temperature PL (LTPL) of DSP and DSBP.

Table 1  
Photophysical properties of DSP and DSBP.

	$E_S$ (eV)	$E_T$ (eV)	$\Delta E_{ST}$ (eV)	HOMO (eV)	LUMO (eV)	$E_g$ (eV)
DSP	2.59	2.48	0.11	-5.64	-2.71	2.93
DSBP	2.64	2.41	0.23	-5.59	-2.68	2.91

Diphenylamine (DPA) units were adopted as the crosslinking unit for the cross-linkable HTM [27]. For the elongated  $\pi$ - $\pi$  conjugations and enhanced hole transporting ability, the phenyl or biphenyl group was introduced into the core of DSP and DSBP, respectively [28]. Fig. 2 shows

the UV-Vis absorbance and photoluminescence (PL) spectra of DSP and DSBP. The optical bandgap ( $E_g$ ) of DSP and DSBP was 2.93 eV and 2.91 eV, respectively. The absorption peaks at 370–380 nm were assigned to the  $\pi$ - $\pi^*$  transitions, originated from the  $\pi$ -conjugations in DSP and DSBP. The shoulder peaks near the wavelength of 310 nm and the absorption profiles less than 400 nm can be attributed to the spirobifluorene species [29,30]. For the steady-state PL spectra, the strong emission peaks centred at 479 and 469 nm corresponding to DSP and DSBP, respectively, were obtained, where the triplet emission for DSP and DSBP were observed at 500 and 514 nm, respectively. The calculated triplet energy values were 2.48 and 2.41 eV for DSP and DSBP, respectively [31,32]. In addition, the HOMO level was estimated through CV as 5.64 and 5.59 eV for DSP and DSBP, respectively, (Fig. S2, supporting information). However, no clear reduction curve was obtained. The LUMO level was calculated to be -2.71 and -2.68 eV from  $E_g$  and HOMO energy level [33,34]. The obtained photophysical, electrochemical, and thermal properties of DSP and DSBP are summarized in Table 1. To investigate the cross-linking temperature and thermal stability properties, the DSC and TGA were conducted as shown in Fig. 3. As displayed in Fig. 3a and b, the crosslinking temperature ranges for DSP and DSBP were 145–175 °C and 154–204 °C, respectively. The two HTMs were cross-linked at temperatures 180 °C, which was well confirmed during the second scan [35]. As shown Fig. 3c and d, DSP and DSBP show high thermal stability at temperature less than 300 °C. Also, the decomposition temperature ( $T_d$ , 5% weight loss) of DSP and DSBP was observed at around 397 °C and 301 °C, respectively [36,37]. The high thermal stability of DSP and DSBP resulted from the rigid structure of spirobifluorene species, which can enhance the light-emitting efficiency of OLEDs [38,39]. As shown in Fig. S3, the FT-IR spectroscopy investigation revealed that DSP and DSBP are well-crosslinked and suitable for application in solution-processed multilayer devices. During

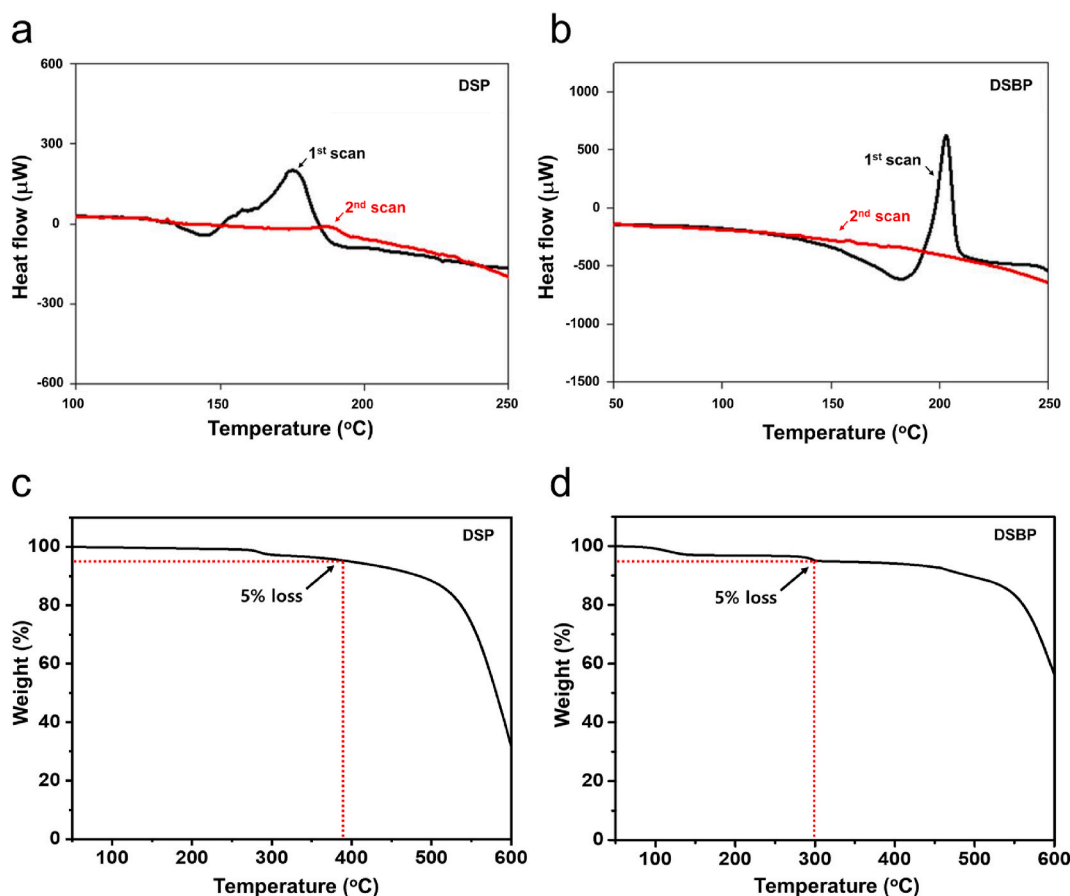


Fig. 3. (a–b) DSC and (c–d) TGA curves of DSP and DSBP, respectively.

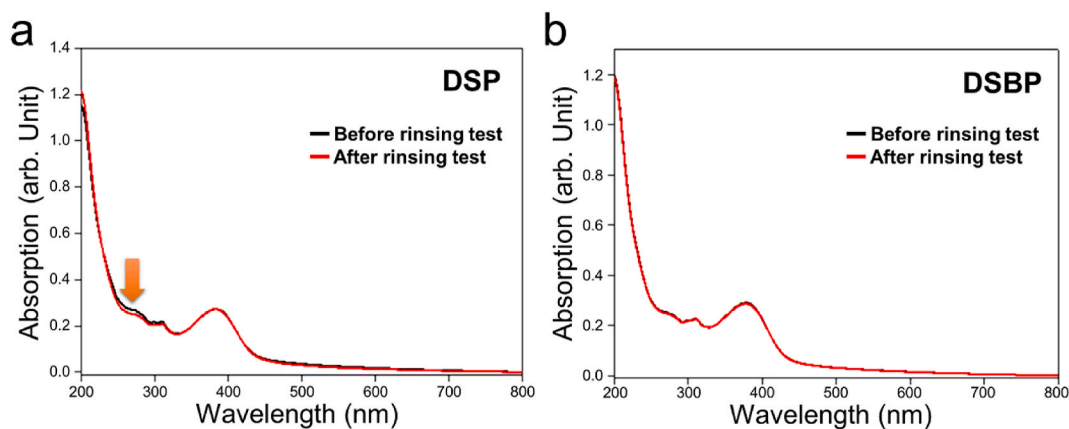


Fig. 4. UV-Vis absorption spectra of DSP and DSBP before and after the rinsing test with the solvent of the EL (toluene).

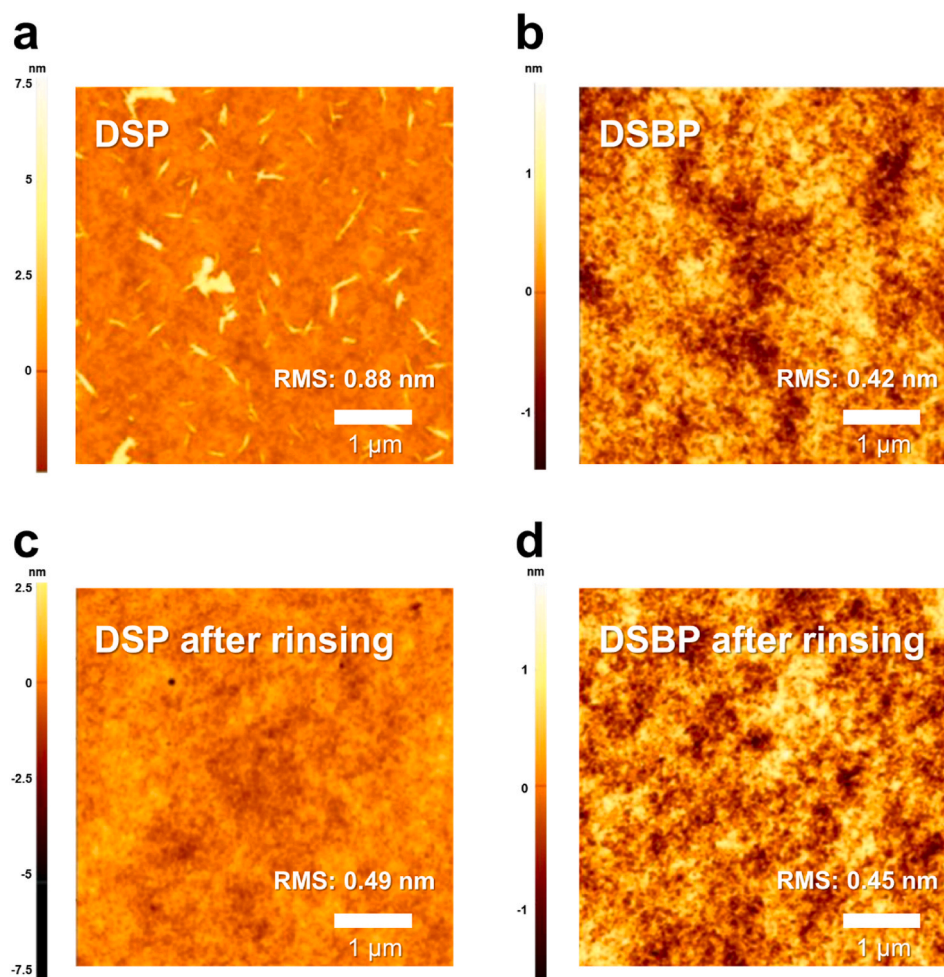
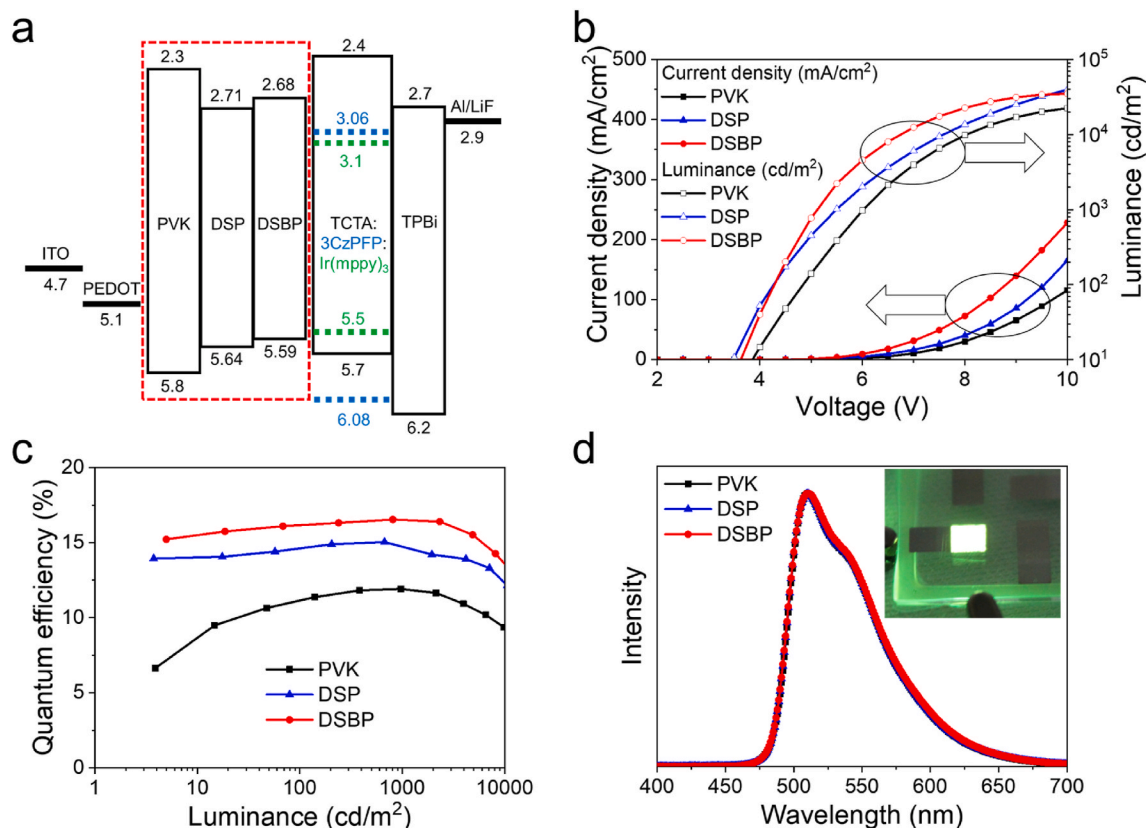


Fig. 5. AFM images of DSP and DSBP before and after the rinsing test with the solvent of the EL (toluene).

thermal crosslinking, the remarkable changes in C=C and C-C bonds could be an evidence of crosslinking, which could be attributed to the conversion of C=C to C-C, observed in the peaks attributed to the styrene units at around  $1681\text{--}1682\text{ cm}^{-1}$ .

The cross-linking properties and feasibility of DSP and DSBP as the HTM in solution processible devices were investigated. The solvent resistance characterization was performed after crosslinking via a rinsing-test using toluene, which was used as the solvent for the EML. For the rinsing-test, the spin-coated DSP and DSBP layers were dried at

$200\text{ }^{\circ}\text{C}$  for 30 min on the hot plate. Subsequently, the HTL samples were rinsed in toluene using a spin-coater at 2000 rpm for 30 s. The UV-Vis absorption spectra of the DSP and DSBP layers were characterized before and after the rinsing test (Fig. 4). After the rinsing-test, a slight decrease in the absorption at a wavelength of 250–300 nm and over 450 nm were observed for DSP. However, no obvious change in the absorption spectra at the entire wavelength was observed for DSBP. This indicates that DSBP has excellent cross-linking property compared to DSP. The AFM topology images reveal the excellent solvent-resistant property of DSBP



**Fig. 6.** Schematic representation of the (a) energy levels, (b) Luminance-voltage-current density, (c) QE-luminance, and (d) electroluminescent characteristics of the fabricated solution-processed OLEDs comprised of PVK, DSP or DSBP as the cross-linkable HTL.

(Fig. 5). For the surface morphology characterization, a Si-wafer was used as a flat substrate. The DSP and DSBP layers were spin-coated on the surface of PEDOT:PSS coated on the Si wafer substrate, followed by the thermal cross-linking treatment. The root-mean-square (RMS) values of the cross-linked films were 0.88 and 0.42 nm for DSP and DSBP, respectively. After the rinsing-test, the RMS value of DSP was significantly reduced to 0.49 nm. However, no obvious change was observed in the RMS value (0.45 nm) of DSBP after the rinsing-test, which well reflects its good solvent-resistive property.

To investigate the performance of the solution-based EL devices with DSP and DSBP, the green phosphorescent organic light-emitting diodes (PHOLEDs) were fabricated with the multi-layered structure as shown in Fig. 6[40]. DSP and DSBP were used for the HTL of the PHOLEDs. To compare the performance of the device, a PHOLED composed of a commercialized polymer, PVK, as the HTL was fabricated. As for the EML, a mixture of 3Cz-PFP and TCTA with a weight ratio of 1:9 was used as the co-host and Ir(mppy)<sub>3</sub> as a dopant in the toluene solvent. All solution processes were conducted by spin-coating. Additionally, considering the triplet energy values of DSP (2.48 eV) and DSBP (2.41 eV), the DSP and DSBP were utilized in the green phosphorescent organic light-emitting diodes (PHOLEDs) [21,41].

TPBi and LiF/Al were deposited on the surface of the EML via the thermal vacuum deposition and the corresponding energy band structures with band alignment are illustrated in Fig. 6a. The current density-voltage and luminance-voltage (IVL) curves and the QE-luminance curves (Fig. 6b and c) indicate that the use of cross-linkable HTLs in EL devices resulted in improved efficiency. As displayed in Fig. 6b, reduced turn-on and operating voltage parameters were obtained by introducing the cross-linkable HTLs. The operating voltages of the EL device with DSBP were 4.3 V at 100 cd/m<sup>2</sup>, 5.1 V at 1000 cd/m<sup>2</sup>, and 6.8 V at 10,000 cd/m<sup>2</sup>. The operating voltages of the EL devices with PVK and DSP were 4.9 and 4.3 V at 100 cd/m<sup>2</sup>, 6.0 and 5.5 V at 1000 cd/m<sup>2</sup>,

**Table 2**

Summary of device performance parameters of OLEDs comprised of PVK, DSP, and DSBP as the HTL.

Devices	Quantum Efficiency (%)		Current Efficiency (cd/A)		Colour coordinate
	Maximum	@1000 cd/m <sup>2</sup>	Maximum	@1000 cd/m <sup>2</sup>	
PVK	11.9	11.9	41.4	41.3	(0.30, 0.62)
DSP	15.0	14.6	47.1	46.7	(0.30, 0.62)
DSBP	16.5	16.1	53.7	53.1	(0.30, 0.62)

and 8.1 and 7.6 V at 10,000 cd/m<sup>2</sup>, respectively. The use of DSBP also resulted in a maximum QE of 16.5% (16.1% QE at 1000 cd/m<sup>2</sup>) compared to the maximum QE of 11.9% (11.9% QE at 1000 cd/m<sup>2</sup>) and maximum QE of 15.0% (14.6% QE at 1000 cd/m<sup>2</sup>) for the EL devices with PVK and DSP as summarized in Table 2. The CE was also enhanced by using the cross-linkable HTLs. The maximum CE parameters were 41.4 cd/A for PVK (41.3 cd/A at 1000 cd/m<sup>2</sup>), 47.1 cd/A for DSP (46.7 cd/A at 1000 cd/m<sup>2</sup>), and 53.7 cd/A for DSBP (53.1 cd/A at 1000 cd/m<sup>2</sup>). As displayed in Fig. 6d, no significant changes in the EL spectra were recorded. The high EL performance of devices with DSP and DSBP resulted from the efficient hole migration and improved interfacial properties of the HTLs. The efficient charge migration through the cross-linkable HTL was evaluated by the fabrication of a hole-only device (HOD) composed of ITO/PEDOT:PSS/HTMs/Au as shown in Fig. S4. The current density values of the HOD with DSBP at the scan voltage were significantly higher than that of the HOD with DSP. The improved current density values can be attributed to the higher hole transporting property of DSBP than DSP [42–44]. The energy band diagram (Fig. 6a) shows that DSP and DSBP can enhance the efficient cascade hole migration from the ITO into the EML. Despite the similar energy level alignment of DSP and DSBP, the EL device with DSBP shows more

outstanding performance than that with DSP. This superior performance is as a result of the enhanced interfacial properties between the HTL and EML, which is due to the outstanding surface morphology and solvent-resistive properties of DSBP.

#### 4. Conclusions

In summary, thermally cross-linkable spirobifluorene-core-incorporated HTLs (DSP and DSBP) were synthesized and used for the fabrication of solution-processible OLEDs. The thermal annealing process for the cross-linking of the HTL was carried out at 180 °C as determined from the DSC and TGA. Via a rinsing-test with an organic solvent used for the EML, we found that DSBP possessed enhanced morphology stability and solvent-resistive property compared with DSP. The synthesized HTLs were used to fabricate OLEDs with the multi-layered structure of ITO glass, HIL, HTL, EML, ETL, and LiF/Al. Considering the charge transporting property of HTL in OLEDs, the appropriate energy levels and triplet energy values of DSP and DSBP promoted the efficient cascade hole migration compared to PVK. As a result, the OLED composed of DSBP had the highest maximum QE of 16.5%, compared to that composed of DSP and PVK with maximum QE of 15 and 11.9%, respectively. Furthermore, the use of DSBP resulted in a lower operating voltage of 5.1 V at 1000 cd/m<sup>2</sup>, compared to the operating voltage observed with the use of DSP and PVK, 5.5 and 6 V, respectively. Hence, with the improved performance of the EL, it was demonstrated that the thermally cross-linkable charge transport layers with the spirobifluorene-core-units can be effectively utilized in various solution-based optoelectronic devices comprising of multi-layered structures.

#### CrediT author statement

Young Eun Kim: Conceptualization, Investigation, Data curation, Writing – original draft. Ara Ko: Conceptualization, Investigation, Data curation, Writing – original draft. Ho Jin Jang: Investigation, Data curation. Sung Joon Yoon: Investigation, Data curation. Seung Hun Roh: Investigation, Data curation. Jun Young Lee: Conceptualization, Investigation. Jun Yeob Lee: Conceptualization, Investigation. Dukjoon Kim: Supervision, Funding acquisition, Writing – review & editing. Jung Kyu Kim: Supervision, Conceptualization, Funding acquisition, Writing – review & editing. Kyoung Soo Yook: Supervision, Conceptualization, Funding acquisition, Writing – review & editing.

#### Declaration of competing interest

The authors declare that they have no known competing financial interests or personal relationships that could have appeared to influence the work reported in this paper.

#### Acknowledgements

The authors acknowledge this work supported by the National Research Foundation of Korea grant funded by the Ministry of Science, ICT & Future Planning, Republic of Korea (NRF-2018M3D1A1058624 and 2019R1F1A1041822), and the MOTIE (Ministry of Trade, Industry & Energy, 10067821) for the development of core technology and components in organic electronics as part of the ICT convergence program for the development of future display devices.

#### Appendix A. Supplementary data

Supplementary data to this article can be found online at <https://doi.org/10.1016/j.dyepig.2020.109122>.

#### References

- [1] Gather MC, Köhnen A, Meerholz K. White organic light-emitting diodes. *Adv Mater* 2011;23(2):233–48. <https://doi.org/10.1002/adma.201002636>.
- [2] Jou J-H, Kumar S, Agrawal A, Li T-H, Sahoo S. Approaches for fabricating high efficiency organic light emitting diodes. *J Mater Chem C* 2015;3(13):2974–3002. <https://doi.org/10.1039/C4TC02495H>.
- [3] Jou J-H, Sahoo S, Dubey DK, Yadav RAK, Swayamprabha SS, Chavhan SD. Molecule-based monochromatic and polychromatic OLEDs with wet-process feasibility. *J Mater Chem C* 2018;6(43):11492–518. <https://doi.org/10.1039/C8TC04203A>.
- [4] Kajjam AB, Vaidyanathan S. Structural mimics of phenyl pyridine (ppy) – substituted, phosphorescent cyclometalated Homo and heteroleptic iridium(III) complexes for organic light emitting diodes – an overview. *Chem Rec* 2018;18(3): 293–349. <https://doi.org/10.1002/tcr.201700035>.
- [5] White MS, Kaltenbrunner M, Glowacki ED, Gutnichenko K, Kettlgruber G, Graz I, et al. Ultrathin, highly flexible and stretchable PLEDs. *Nat Photon* 2013;7(10): 811–6. Go to ISI>://WOS:000325003100015.
- [6] Kaltenbrunner M, White MS, Glowacki ED, Sekitani T, Someya T, Sariciftci NS, et al. Ultrathin and lightweight organic solar cells with high flexibility. *Nat Commun* 2012;3. Go to ISI>://WOS:000303455200007.
- [7] Eritt M, May C, Leo K, Toerker M, Radehaus C. OLED manufacturing for large area lighting applications. *Thin Solid Films* 2010;518(11):3042–5. <https://doi.org/10.1016/j.tsf.2009.09.188>.
- [8] Jou J-H, Su Y-T, Liu S-H, He Z-K, Sahoo S, Yu H-H, et al. Wet-process feasible candlelight OLED. *J Mater Chem C* 2016;4(25):6070–7. <https://doi.org/10.1039/C6TC01968D>.
- [9] Chen J-X, Tao W-W, Chen W-C, Xiao Y-F, Wang K, Cao C, et al. Red/near-infrared thermally activated delayed fluorescence OLEDs with near 100 % internal quantum efficiency. *Angew Chem Int Ed* 2019;58(41):14660–5. <https://doi.org/10.1002/anie.201906575>.
- [10] Liang J, Li C, Cui Y, Li Z, Wang J, Wang Y. Rational design of efficient orange-red to red thermally activated delayed fluorescence emitters for OLEDs with external quantum efficiency of up to 26.0% and reduced efficiency roll-off. *J Mater Chem C* 2020;8(5):1614–22. <https://doi.org/10.1039/C9TC05892C>.
- [11] Bae WK, Lim J. Nanostructured colloidal quantum dots for efficient electroluminescence devices. *Kor J Chem Eng* 2019;36(2):173–85. <https://doi.org/10.1007/s11814-018-0193-7>.
- [12] Kim JK, Kim W, Wang DH, Lee H, Cho SM, Choi D-G, et al. Layer-by-Layer all-transfer-based organic solar cells. *Langmuir* 2013;29(17):5377–82. <https://doi.org/10.1021/la400137g>.
- [13] Song YJ, Kim J-W, Cho H-E, Son YH, Lee MH, Lee J, et al. Fibertronic organic light-emitting diodes toward fully addressable, environmentally robust, wearable displays. *ACS Nano* 2020;14(1):1133–40. <https://doi.org/10.1021/acsnano.9b09005>.
- [14] Abbel R, de Vries I, Langen A, Kirchner G, t'Mannetje H, Gorter H, et al. Toward high volume solution based roll-to-roll processing of OLEDs. *J Mater Res* 2017;32(12):2219–29. <https://doi.org/10.1557/jmr.2017.204>.
- [15] Jung E, Kim C, Kim M, Chae H, Cho JH, Cho SM. Roll-to-roll preparation of silver-nanowire transparent electrode and its application to large-area organic light-emitting diodes. *Org Electron* 2017;41:190–7. <https://doi.org/10.1016/j.orgel.2016.11.003>.
- [16] Wang S, Zhang H, Zhang B, Xie Z, Wong W-Y. Towards high-power-efficiency solution-processed OLEDs: material and device perspectives. *Mater Sci Eng R Rep* 2020;140:100547. <https://doi.org/10.1016/j.mser.2020.100547>.
- [17] Dubey DK, Swayamprabha SS, Kumar Yadav RA, Tavgeniene D, Volyniuk D, Grigalevicius S, et al. A thermally cross-linkable hole-transporting small-molecule for efficient solution-processed organic light emitting diodes. *Org Electron* 2019; 73:94–101. <https://doi.org/10.1016/j.orgel.2019.06.011>.
- [18] Limberg FRP, Schneider T, Höfle S, Reisbeck F, Janietz S, Colmann A, et al. 1-Ethynyl ethers as efficient thermal crosslinking system for hole transport materials in OLEDs. *Adv Funct Mater* 2016;26(46):8505–13. <https://doi.org/10.1002/adfm.201603862>.
- [19] Kang YJ, Bail R, Lee CW, Chin BD. Inkjet printing of mixed-host emitting layer for electrophosphorescent organic light-emitting diodes. *ACS Appl Mater Interfaces* 2019;11(24):21784–94. <https://doi.org/10.1021/acsaami.9b04675>.
- [20] Yan H, Lee P, Armstrong NR, Graham A, Evmenenko GA, Dutta P, et al. High-performance hole-transport layers for polymer light-emitting diodes. Implementation of organosiloxane cross-linking chemistry in polymeric electroluminescent devices. *J Am Chem Soc* 2005;127(9):3172–83. <https://doi.org/10.1021/ja044455q>.
- [21] Park S-R, Kang J-H, Ahn DA, Suh MC. A cross-linkable hole transport material having improved mobility through a semi-interpenetrating polymer network approach for solution-processed green PHOLEDs. *J Mater Chem C* 2018;6(29): 7750–8. <https://doi.org/10.1039/C8TC01435C>.
- [22] Kim JH, Hwang S-H, Song W, Lee JY. Acridine modified dibenzothiophene derivatives as high triplet energy host materials for blue phosphorescent organic light-emitting diodes. *Dyes Pigments* 2015;122:103–8. <https://doi.org/10.1016/j.dyepig.2015.06.014>.
- [23] Lee CW, Lee JY. Above 30% external quantum efficiency in blue phosphorescent organic light-emitting diodes using pyrido[2,3-b]indole derivatives as host materials. *Adv Mater* 2013;25(38):5450–4. <https://doi.org/10.1002/adma.201301091>.
- [24] Yang J, Qin J, Ren Z, Peng Q, Xie G, Li Z. Pyrene-based blue AIEgen: enhanced hole mobility and good EL performance in solution-processed OLEDs. *Molecules* 2017; 22(12):2144. <https://www.mdpi.com/1420-3049/22/12/2144>.

- [25] Liu H, Bai Q, Yao L, Zhang H, Xu H, Zhang S, et al. Highly efficient near ultraviolet organic light-emitting diode based on a meta-linked donor–acceptor molecule. *Chem Sci* 2015;6(7):3797–804. <https://doi.org/10.1039/C5SC01131K>.
- [26] Patil VV, Lee KH, Lee JY. Isomeric fused benzocarbazole as a chromophore for blue fluorescent organic light-emitting diodes. *J Mater Chem C* 2020;8(24):8320–7. <https://doi.org/10.1039/D0TC01268H>.
- [27] Aizawa N, Pu Y-J, Sasabe H, Kido J. Thermally cross-linkable host materials for enabling solution-processed multilayer stacks in organic light-emitting devices. *Org Electron* 2013;14(6):1614–20. <https://doi.org/10.1016/j.orgel.2013.03.028>.
- [28] Cho YJ, Lee JY. Low driving voltage, high quantum efficiency, high power efficiency, and little efficiency roll-off in red, green, and deep-blue phosphorescent organic light-emitting diodes using a high-triplet-energy hole transport material. *Adv Mater* 2011;23(39):4568–72. <https://doi.org/10.1002/adma.201102045>.
- [29] Karim MA, Cho Y-R, Park JS, Yoon K-J, Lee SJ, Jin S-H, et al. Synthesis and characterization of spirobifluorene-based polymers for organic light-emitting diode applications. *Macromol Res* 2008;16(4):337–44. <https://doi.org/10.1007/BF03218526>.
- [30] Wu F-I, Shu C-F, Wang T-T, Diao EW-G, Chien C-H, Chuen C-H, et al. Bis(2,2-diphenylvinyl)spirobifluorene: an efficient and stable blue emitter for electroluminescence applications. *Synth Met* 2005;151(3):285–92. <https://doi.org/10.1016/j.synthmet.2005.06.003>.
- [31] Jeong SH, Jang HJ, Lee JY. High triplet energy crosslinkable hole transport material for blue phosphorescent organic light-emitting diodes. *J Ind Eng Chem* 2019;78:324–9. <https://doi.org/10.1016/j.jiec.2019.05.038>.
- [32] Jung M, Lee KH, Lee JY, Kim T. A bipolar host based high triplet energy electroplex for an over 10 000 h lifetime in pure blue phosphorescent organic light-emitting diodes. *Materials Horizons* 2020;7(2):559–65. <https://doi.org/10.1039/C9MH01268K>.
- [33] Konidena RK, Chung WJ, Lee JY. C1-, C2-, and C3-modified carbazole derivatives as promising host materials for phosphorescent organic light-emitting diodes. *Org Lett* 2020;22(7):2786–90. <https://doi.org/10.1021/acs.orglett.0c00767>.
- [34] Li Z, Jiao B, Wu Z, Liu P, Ma L, Lei X, et al. Fluorinated 9,9'-spirobifluorene derivatives as host materials for highly efficient blue organic light-emitting devices. *J Mater Chem C* 2013;1(11):2183–92. <https://doi.org/10.1039/C3TC00466J>.
- [35] Park S-M, Yook K-S, Lee W-H, Hong Y, Lee J-Y, Kang I-N. Synthesis and characterization of thermally crosslinkable hole-transporting polymers for PLEDs. *J Polym Sci Polym Chem* 2013;51(23):5111–7. <https://doi.org/10.1002/pola.26943>.
- [36] Kwak J, Lyu Y-Y, Lee H, Choi B, Char K, Lee C. New carbazole-based host material for low-voltage and highly efficient red phosphorescent organic light-emitting diodes. *J Mater Chem* 2012;22(13):6351–5. <https://doi.org/10.1039/C2JM15138C>.
- [37] Konidena RK, Lee Kh, Lee JY, Hong WP. A new benzothienindole-based bipolar host material for efficient green phosphorescent organic light-emitting diodes with extremely small efficiency roll-off. *Org Electron* 2019;70:211–8. <https://doi.org/10.1016/j.orgel.2019.04.006>.
- [38] Bian M, Wang Y, Guo X, Lv F, Chen Z, Duan L, et al. Positional isomerism effect of spirobifluorene and terpyridine moieties of “(A)n–D–(A)n” type electron transport materials for long-lived and highly efficient TADF-PhOLEDs. *J Mater Chem C* 2018; 6(38):10276–83. <https://doi.org/10.1039/C8TC03796E>.
- [39] Kwak K, Cho K, Kim S. Analysis of thermal degradation of organic light-emitting diodes with infrared imaging and impedance spectroscopy. *Optic Express* 2013;21 (24):29558–66. <https://doi.org/10.1364/OE.21.029558>.
- [40] He X, Cai D, Kang D-Y, Haske W, Zhang Y, Zuniga CA, et al. Phosphorescent light-emitting diodes using triscarbazole/bis(oxadiazole) hosts: comparison of homopolymer blends and random and block copolymers. *J Mater Chem C* 2014;2 (33):6743–51. <https://doi.org/10.1039/C4TC01079E>.
- [41] Wang Y. Dramatic effects of hole transport layer on the efficiency of iridium-based organic light-emitting diodes. *Appl Phys Lett* 2004;85(21):4848–50. <https://doi.org/10.1063/1.1823031>.
- [42] Yang Y, Yang X, Yang W, Li S, Xu J, Jiang Y. Ordered and ultrathin reduced graphene oxide LB films as hole injection layers for organic light-emitting diode. *Nanoscale Research Letters* 2014;9(1):537. <https://doi.org/10.1186/1556-276X-9-537>.
- [43] Moon JS, Ahn DH, Kim SW, Lee SY, Lee JY, Kwon JH.  $\delta$ -Carboline-based bipolar host materials for deep blue thermally activated delayed fluorescence OLEDs with high efficiency and low roll-off characteristic. *RSC Adv* 2018;8(31):17025–33. <https://doi.org/10.1039/C8RA01761A>.
- [44] Neophytou M, Griffiths J, Fraser J, Kirkus M, Chen H, Nielsen CB, et al. High mobility, hole transport materials for highly efficient PEDOT:PSS replacement in inverted perovskite solar cells. *J Mater Chem C* 2017;5(20):4940–5. <https://doi.org/10.1039/C7TC00858A>.